IEEE Access
Multidisciplinary | Rapid Review | Open Access Journal

Received 16 May 2024, accepted 8 June 2024, date of publication 17 June 2024, date of current version 27 June 2024.

Digital Object Identifier 10.1109/ACCESS.2024.3415507

RESEARCH ARTICLE

Closed-Loop Current Control of a SiC-Based Power Converter via Galvanically Isolated Electroluminescence Sensing

JOENY S. ZHEN[1], (Student Member, IEEE), KEITH A. CORZINE[1], (Fellow, IEEE), MATTHEW A. PORTER[2], (Student Member, IEEE), AND TODD R. WEATHERFORD[2], (Senior Member, IEEE)

[1]Department of Electrical and Computer Engineering (ECE), University of California at Santa Cruz, Santa Cruz, CA 95064, USA
[2]Naval Postgraduate School, Monterey, CA 93943, USA

Corresponding author: Joeny S. Zhen (jozhen@ucsc.edu)

This work was supported in part by the U.S. Navy Capt. (Ret.) Lynn (LJ) Petersen at the Office of Naval Research under Grant N00014-21-1-2260.

ABSTRACT Electromagnetic interference poses enormous challenges for feedback-controlled systems, especially at medium-voltage levels. As power converters are increasingly utilized for medium- and high-voltage applications, optically-based measurement methods must be explored. This paper investigates current measurement via electroluminescence from silicon carbide semiconductor devices. A SiC half-bridge MOSFET module, provided by Powerex, is manufactured with fiber optic cables placed against the semiconductor junctions. The new fiber ports are employed to characterize the light spectrum as a function of conducted current and junction temperature for the body diodes. Most of the light energy is concentrated around peaks at 390 nm and 500 nm. It is observed that although the energy at the 390 nm peak increases with rising temperature, the energy at the 500 nm peak decreases. Therefore, the total light output is seen to only slightly vary with temperature and mostly depends on conducted current. A function is fitted to the light transducer output as a in relation to the on-state current. This function is utilized in a microprocessor that implements feedback current control in a buck converter. This type of control forms the basis of torque regulation in a motor drive or an ''inner-current loop'' of motor drive speed control or converter voltage control. The new electroluminescence control was demonstrated in the laboratory on a prototype system where the current command is stepped from 0 to 25A, showcasing the effectiveness of the new optical sensing method.

INDEX TERMS Converter control, DC-DC converters, electroluminescence, silicon carbide (SiC).

I. INTRODUCTION

Switching power converters find wide application in photovoltaic systems [1], [2], switched-mode power supplies [3], wind-energy conversion systems [4], battery charging, electric vehicle applications [5], etc. Moreover, there is a trend towards medium-voltage operation requiring exceptional electromagnetic compatibility (EMC). Silicon-carbide (SiC) semiconductor devices are gaining traction in modern applications due to superior thermal properties [6]. The rapid switching times of wide bandgap (WBG) semiconductors leads to mitigation of transistor switching losses and diode reverse recovery, which increases efficiencies and greatly improves thermal management [10]. The exceptional thermal conductivity of WBG devices, particularly SiC, simplifies thermal management design, resulting in a reduction in overall weight. This is particularly evident in applications where power density is critical, such as all-electric aircraft [11] and Naval ship propulsion [12], [14]. Petersen and Ericsen have outlined the future of power energy systems and US naval

The associate editor coordinating the review of this manuscript and approving it for publication was Md. Rabiul Islam.

systems [13], which emphasized 2 to 4 increases in power density while reducing conversion losses by 50% using SiC and increased switching frequency. Although costs may be higher now, 6'' wafer production promises to reduce SiC costs to that of Si or below for equivalent power capabilities [15].

Due to faster switching at higher voltages provided by SiC, EMC is prevalent and can adversely affect nearby devices [16]. EMC can affect the performance and reliability of switching converters that incorporate closed-loop feedback control. This paper focuses on an optical method of measuring on-state current of a SiC semiconductor in a power converter. The current measurement is fed into a proportional-plus-integral (PI) regulated current control, which is a standard structure for motor drives, active rectifiers, dc/dc converters, etc.; sometimes as a supervisory control and other times as an ''inner current loop''. The classical current control is implemented in the proposed optical method shown in Figure 1.

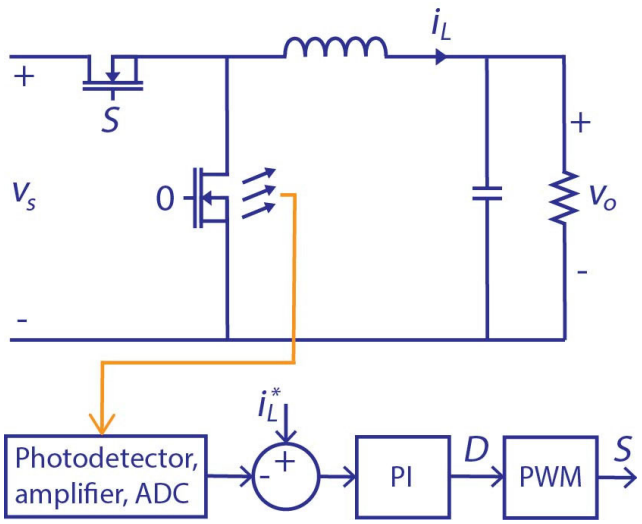

FIGURE 1. Structure of a common feedback control implemented with optical method measuring on-state current of a SiC MOSFET.

In Figure 1, the PI control commands a duty cycle D in order to control a current to its commanded value. The output S is the PWM signal for the upper MOSFET, while the bottom MOSFET is gated off.

EMC Concerns in Power Converters: Rapid transistor switching in medium-voltage applications leads to significant noise generation through sensitive components such as gate drivers and sensors - resulting in degraded reliability and potential catastrophic failures [17]. The points at which noise is most prevalent are wires and PCB traces where pulsating magnetic flux caused by high di/dt injects high frequency noise, where any capacitive coupling establishes a path to high frequency currents caused by high dv/dt. To mitigate this, the most common approach is to ''slow down'' the switching performance by increasing the gate resistance of the drive circuitry, which in return, negates the benefits of fast switching from WBGs [18]. A better approach is to eliminate or minimize wires, wire-loops, and PCB traces from the driving and sensing circuitry located in proximity to electrically connected high dv/dt nodes. A promising solution is wireless data transfer through isolation [19], [20], [21], [22]. Transformer isolation leads to bulky and heavy components making that a less-desirable solution considering high-power density requirements. In power electronics that incorporate feedback control systems, such as those employed in current-loop control [43], sensing is typically done through hall-effect sensors. Recent research [44] has demonstrated that hall-effect sensors are dramatically affected by EMI presence. Numerous tests ranging from Bulk-Current Injection (BCI), Transverse-Electromagnetic cell (TEM), and Direct Power Injection (DPI) experiments were demonstrated to prove that reliability and accuracy of hall-effect sensors degrades in the presence of EMI, especially where it is most prevalent in medium-voltage levels (1-100 kV). Thus, other forms of isolation and contact-less sensing are required.

Fiber optics are generally preferred and inexpensive due to their wide range of applications. Fibers are immune to EMC issues [23]. In addition, light is composed of photons, so it cannot be affected by EMC in a traditional sense. The work herein is based on optical fiber-coupled electroluminescence from WBG semiconductors which has been demonstrated in recent work [24], [25], [26], [27], [28], [29]. In [24], the authors detail findings and characteristics of electroluminescence from a GaN power diode. Subsequently, [26] details the development of a closed-loop DC-DC buck converter that incorporates GaN electroluminescence to control the system's current. In [27], [28], and [29], the authors characterized SiC electroluminescence, and propose the use of a neutral network to predict current and temperature of the system from SiC EL.

II. ELECTROLUMINESCENCE FROM SILICON CARBIDE

For this work, a custom half-bridge module that incorporates GeneSiC 3.3 kV 50A MOSFETs with fiber ports was developed by Powerex. The SiC MOSFET from GeneSiC is G2R50MT33-CAL. A design drawing of the module is shown in Figure 3. As can be seen, additional fibers are added and placed up against the MOSFET and diode dies. SiC EL depends on the conducted current and temperature of the die [24]. The general spectral dependence of excitonic electroluminescence is given by the formula

$$I_x(h\omega) \propto I^n \left(h\omega - E_x(T)\right) \gamma \cdot e^{h\omega - E_x(T)/kT} \tag{1}$$

Here, $E_X(T)$ represents the exciton energy, I represents the current magnitude, and T is the local temperature [25]. The variable h is Planck's constant, ω is the angular frequency, k is the wave number, n is the number of photons, and γ is the short-range spin exchange interaction in meV. The exciton energy shifts to lower energy as the temperature increases due to the shift in the bandgap energy, as given by the Varshini equation

$$E_x(T) = E_x(0) - \frac{\alpha T}{T^2 + \beta} \tag{2}$$

where E_X (0) is the bandgap energy of the material at a temperature of 0 K, and α and β are semiconductor-dependent constants. Figure 2 displays the circuit schematic used for observing SiC EL. The bottom MOSFET's body diode was forward biased with current, I_{Sweep}. Figure 3 shows the CAD diagram of the Powerex MOSFET module and Figure 4 shows SiC EL from inside the module running at 30A during forward conduction of the internal body diode and is caused by radiative recombination at the PN-junction [27]; a phenomenon discovered [30] and reported in subsequent investigations [31].

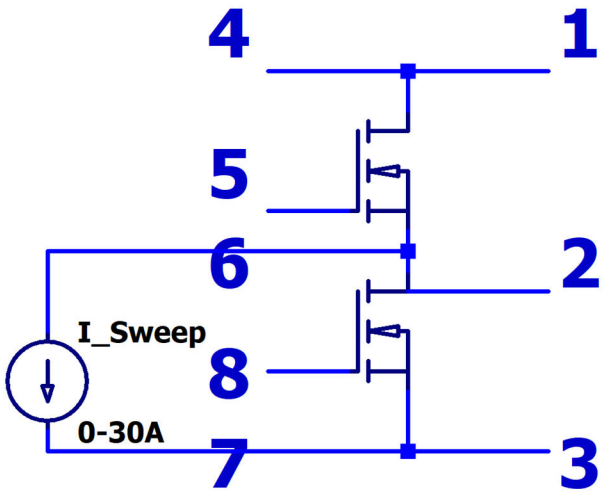

FIGURE 2. Circuit schematic for forward biasing the lower MOSFET body diode during EL test.

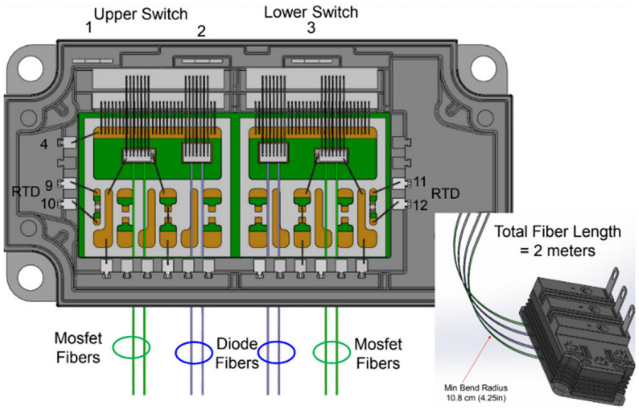

FIGURE 3. SiC half-bridge power module (3.3kV/50A) from PowerEx.

The corner view of the experimental setup is shown in Figure 5. It is composed of a SiC half-bridge module, a cold plate for liquid cooling, and fibers to measure SiC electroluminescence. The fibers are connected to an Ocean Insights HR4000 CG-UV-NIR spectrometer to investigate and characterize the spectra of the SiC MOSFET body diode's EL dependency on current and temperature. Figure 13 is provided to illustrate the top-view of the setup.

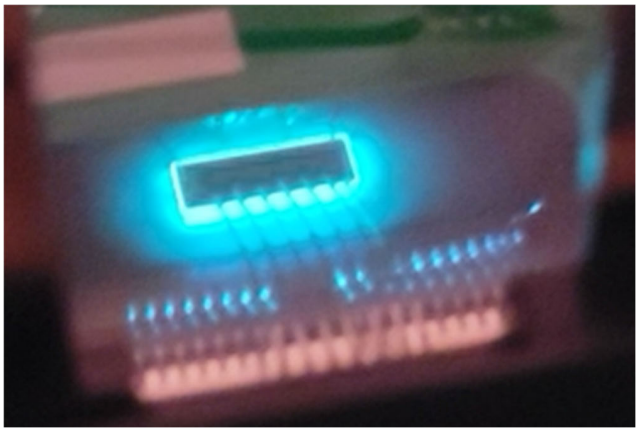

FIGURE 4. Electroluminescence of SiC MOSFET body diode with the package lid removed.

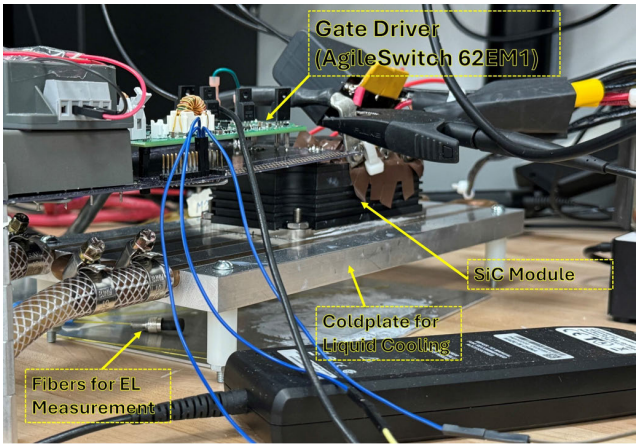

FIGURE 5. Corner view of SiC EL experimental setup.

A. SiC ELECTROLUMINESCENCE CURRENT DEPENDENCY

The SiC MOSFET body diode's EL spectra was obtained while performing a current sweep - from 7.5A to 30A. The circuit schematic is shown in Figure 2. A constant case temperature of 20 ^{o}C was maintained through liquid cooling to ensure the data captured in the second study only exhibits current dependency. The SiC EL spectra dependency on current is shown in Figure 7.

Since SiC is an indirect bandgap semiconductor, nonradiative electron-hole recombination is dominant [32], resulting in a low emission of radiative recombination [27]. This was observed in the second study, as light was not visible at the end of the fiber until the body diode was subjected to 5A of current - as higher current densities increase radiative recombination. The integration time was set to 30 seconds to allow the spectrometer's ADC to compensate for low light emission. This integration time increases the noise in the spectra capture shown in Figure 7.

These measurements were compared to previous studies of a GaN diode. The GaN device light amplitude (counts) was approximately 2250 times more than the SiC setup [24], [26].

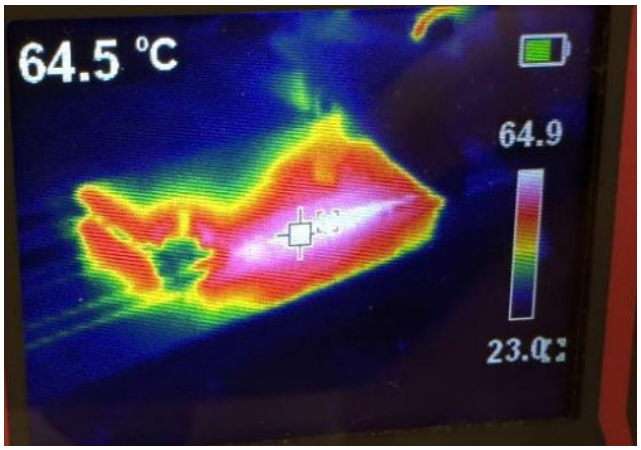

FIGURE 6. Corner view thermal image of SiC module at 64.5 °C.

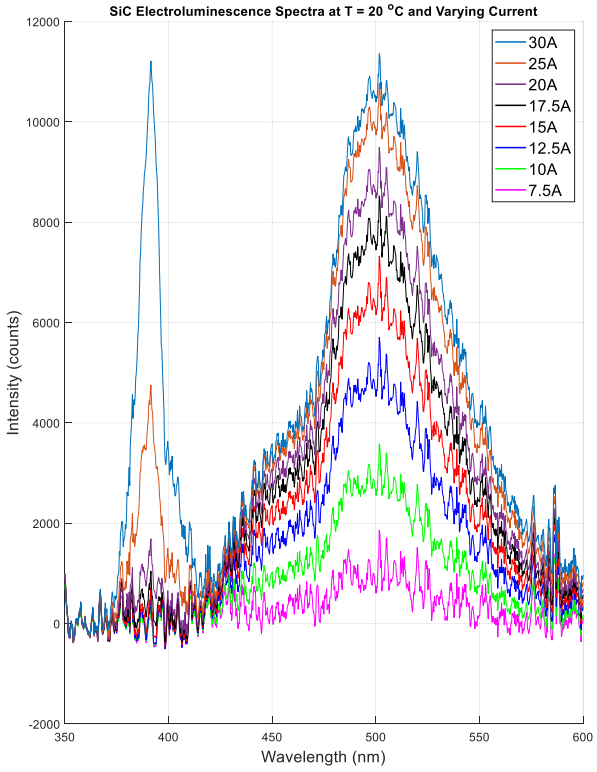

FIGURE 7. Electroluminescence spectra of SiC MOSFET body diode for varying temperatures at constant current.

There are two dominant spectral peaks - one at 390 nm and another at 500 nm. The primary peak at 500 nm seen at all current ranges also contains a side lateral peak at 460 nm which exhibits the same behavior as the primary peak. The intensity of the primary peak and its side lateral peak results from deep recombination centers formed by boron dopant atoms. The recombination center enables radiative donor-acceptor recombination with shallow donor levels related to nitrogen dopants [27], [28], [29] [33], [34], [35], [36]. The secondary peak at 390 nm is due to band-edge

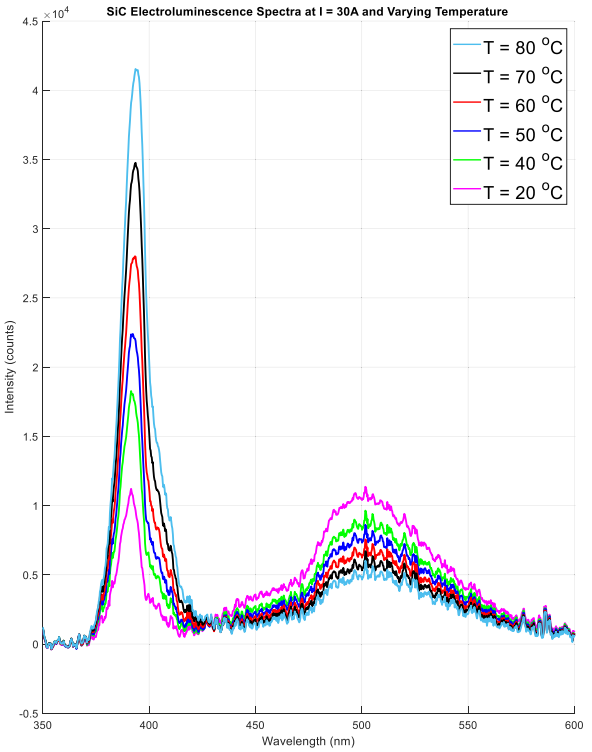

FIGURE 8. Electroluminescence spectra of SiC MOSFET body diode with constant temperature and varying current.

recombination at a bandgap energy of 3.2 eV [27], [28], [29], [37], [38]. Note that the 390 nm peak was not observed at an integration time of 30s until around 20A as seen in Figure 7. Upon observation, it is noted that, at a constant temperature of 20 °C, the light intensity at the major peaks increases with rising current - which is to be expected. The current dependency is due to the number of minority carriers that are injected into the PN-junction to increase radiative electron-hole recombination [27], [28], [29].

B. SiC ELECTROLUMINESCENCE TEMPERATURE DEPENDENCY

Dependency on temperature is seen by setting the power supply in constant current mode and operating the device at 30A. The junction temperature was varied by running the device without any cooling while the temperature was measured with a thermal imaging camera as highlighted in Figure 6. Data was captured at 10 °C intervals starting at 40 °C. The spectra of 30A at 20 °C is also provided as a reference. The SiC EL spectra dependency on temperature is shown in Figure 7. Figure 6 illustrates a corner view of the setup on how temperature was measured using a thermal imaging camera. In this case, the example captures the junction temperature at 64.5 °C.

As seen in Figure 8, the two dominant peaks at 390 nm and 500 nm exhibit opposing dependencies with temperature. With rising junction temperature, the 500 nm peak decreases while the 390 nm peak increases. The peak reduction at

500 nm is explained by increasing thermal ionization of the donor level [33], [39]. As more electrons are ionized to the conduction band, the probability for donor-acceptor recombination decreases as the density of the donor states falls. This explains why there is a counteracting influence of the two major peaks, also seen in experimental setups [27], [28], [29].

C. CHARACTERIZATION OF SiC ELECTROLUMINESCENCE SPECTRA

Upon observation of Figures 7 and 8, the current and temperature have an interacting influence on the 390 nm peak where they both increase the light intensity. Whereas current and temperature counteract on the 500 nm peak where current increases light intensity while temperature decreases it. Therefore, at 390 nm, the peak at its maximum is achieved through maximum current and temperature. At 500 nm, the peak at its maximum is achieved through maximum current and minimum temperature.

The results of the SiC MOSFET body diode electroluminescence spectra verify its dependence on current and junction temperature. This serves as motivation to use SiC EL for current and temperature sensing to develop a feedback control using these parameters to regulate a switching converter. This approach would be a possible alternative to using hall effect sensors in a high EMI environment. It is noted that these two influences are superimposed upon each other during regular operation. Due to this, a single intensity measurement will not sufficiently extract both current and temperature data accurately. For instance, when measuring the entire SiC EL spectrum using a photodiode or photodetector, a change in current will change the SiC EL intensity, which will change photodiode current - as identified in Figures 7 and 8 where an increase in current increases overall spectrum intensity. However, the temperature will not affect the overall SiC EL intensity - this is identified in an equal and opposite change in area for the two major peaks [28]. This results in a net-neutral intensity during a change in temperature when measuring overall spectra. Temperature can be predicted from SiC EL if filtered through a 390 nm or a 500 nm bandpass filter. To control current in a buck converter implementing SiC EL, the simplest approach would be measuring the overall SiC EL spectra. One thing to note is to predict the temperature of SiC without a thermocouple, filtering SiC EL through a 390 nm or a 500 nm bandpass filter and comparing the intensity measurement to a set baseline intensity value at room temperature is possible.

III. OPEN-LOOP CALIBRATION

An avalanche photodiode (APD) transducer was chosen for this work. APDs have a larger noise floor due to avalanche noise, but they typically have better SNR due to their higher gains. In addition, APDs do behave nonlinearly at higher gains, which requires accurate calibration for SiC EL over a range of operating current and temperature.

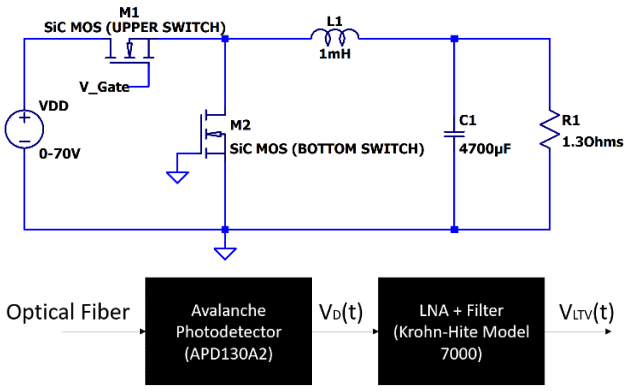

FIGURE 9. SiC EL buck converter open-loop calibration setup.

A. CALIBRATION OF AN APD

An avalanche photodetector explores calibrating a SiC EL signal to an electrical signal. The APD used is a Thorlabs APD130A2. The goal is to observe the light to electrical signal performance. This is done by putting together a simple buck converter - taking advantage of the half-bridge topology of the module. The upper switch was used as the primary switch of the buck converter. The bottom switch was disabled by shorting the gate-to-source voltage such that the off cycle current runs through the body diode. This is done while keeping the case temperature constant at 20 ^{o}C. The buck converter was run via open loop at a switching frequency of 100 kHz and a duty cycle of 50%. A LAUNCHPADXL-F28379D microcontroller was used to generate the gate signals. The gate driver used in this setup was the AgileSwitch 62EM1. Figure 9 displays the circuit schematic diagram of the fourth study.

Figure 10 displays the SiC EL measured by an APD of the buck converter running at 10A of current via open loop. The first waveform shows the inductor current. The second waveform, $V_D(t)$, is the output of the APD measuring SiC EL of the MOSFET body diode. The third waveform, $V_{LTV}(t)$, is a filtered and amplified version of the APD measuring SiC EL. Recall that APDs have higher noise floor due to avalanche noise - explaining the noise on the second plot. In addition, due to the nature of SiC being an indirect bandgap material, the light going into the transducer is very weak in intensity, despite the high gain of the APD. To compensate, an additional low-noise amplifier was used as well. This would also increase the SNR as seen in the third trace. The cutoff frequency of the filter was set to 400 kHz and the gain of the amplifier was set to 100. Calibration was done by running the converter at 50% duty cycle open-loop and mapping a point along the inductor current where the system is triggered by a falling edge signal as seen in Figure 10. Numerous points were obtained manually by sweeping the current from 2-30A. Although the calibration is done manually, it can be performed automatedly with an algorithm. The measured current vs EL was plotted as shown in Figure 11.

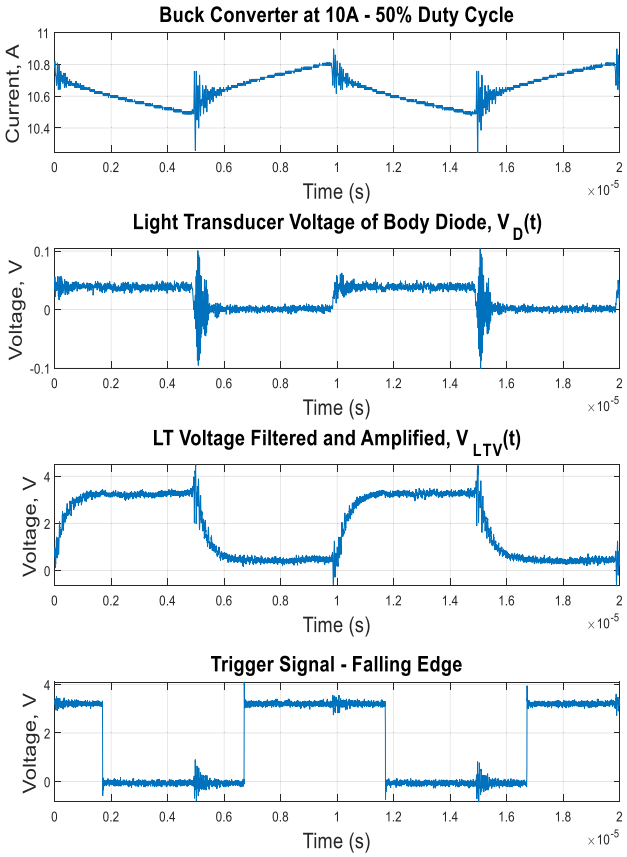

FIGURE 10. Open-loop converter test for EL of SiC MOSFET.

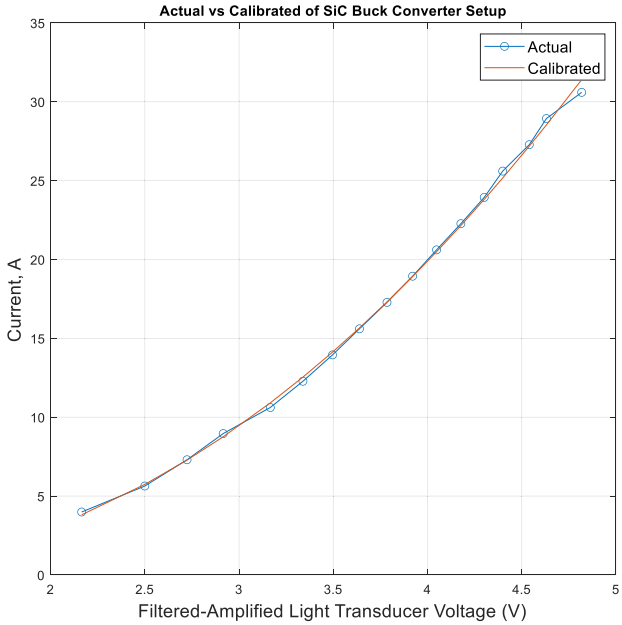

FIGURE 11. Actual vs calibrated current of SiC EL buck converter setup (OL).

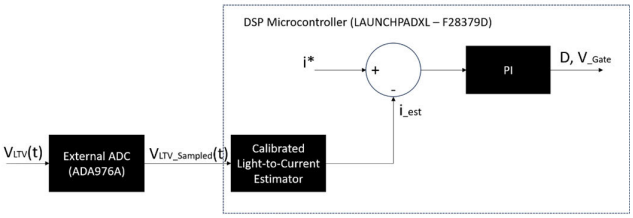

FIGURE 12. Buck converter SiC closed-loop control setup schematic.

Therein, the non-linear nature of the APD is noted as current is swept from 2-30A.

A polynomial fit was obtained via least-squares approximation. The calibration equation that closely matches the open-loop experimental result, with an order of 2 and a minimized norm of 1.1514, is

$$\hat{i} = 2.0029V_{LTV}^2 - 3.5878V_{LTV} + 2.1919 \qquad (3)$$

IV. BUCK CONVERTER CLOSED-LOOP CURRENT CONTROL

A closed-loop control system utilizing a SiC MOSFET body diode EL was digitally implemented. The filtered-amplified light transducer voltage is sent to an external analog-to-digital converter (ADC), allowing the conversion of this voltage back to a current value based on (3). In this setup, an external ADC, specifically the AD976A, was employed instead of the onboard ADC of the microcontroller. This choice was made to benefit from larger bit resolution, accommodate the filtered-amplified electrical signal of SiC EL with a larger acceptable input signal range, and achieve faster conversion speeds.

To ensure precise sampling, the external ADC was triggered at a specific point in every cycle of the amplified-filtered light transducer voltage signal. This approach avoids sampling during periods when the diode is off, ensuring accurate data acquisition and enabling the development of a relationship between voltage and current, as depicted in (3). Figure 10 visually represents the trigger signal in the bottom trace, illustrating that samples are taken at every falling edge of the signal cycle.

This was calculated in the DSP microcontroller, resulting in i_{est}. The estimated current is subtracted from a commanded current, i*, to determine the error between the two values. The error is sent into a PI controller, where, with carefully selected gains which can be determined via Ziegler-Nichols method [41], outputs a duty cycle to control the system current that minimizes the error. Figure 12 shows the PI control scheme for the circuit and Figures 13 shows the photo of the setup.

Results of the closed-loop current control are shown in Figures 14 and 15. A step response of 0 to 25A was performed by changing the commanded value, i*. The supply voltage was set to 60V for this experiment. Figure 14 displays the experimental results of the 0-25A step response. The PI gains set are $K_P = 0.001$ and $K_I = 2$. For a 5.5A step, the system reached steady-state in around 1s. For a 15A step, the system

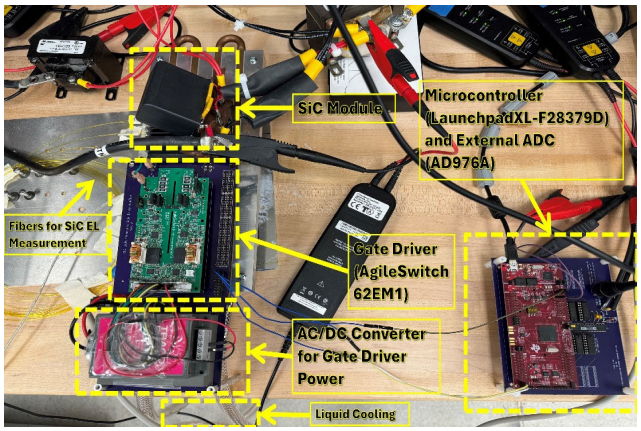

FIGURE 13. Buck converter SiC EL setup for open-loop and closed-loop control.

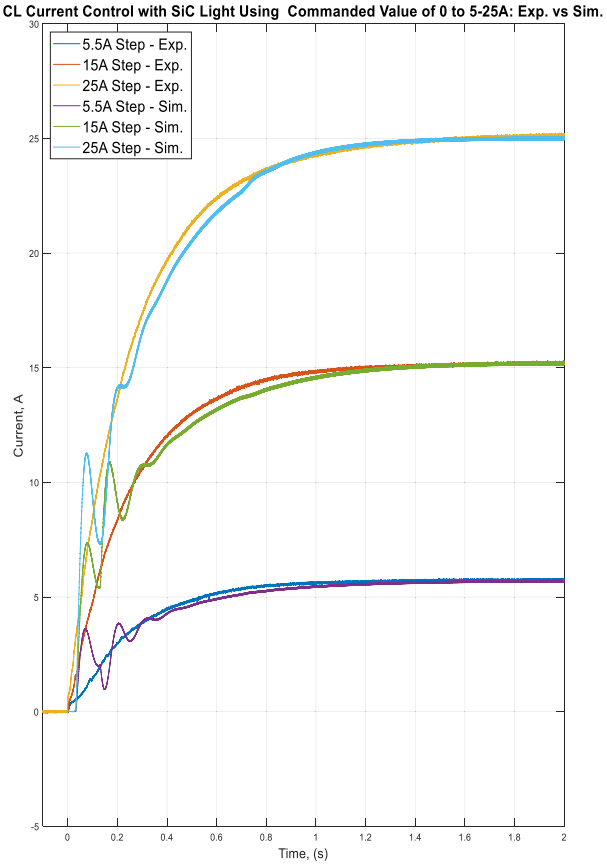

FIGURE 14. Step response of closed-loop current control based on EL current measurement: experimental vs simulated.

reached steady-state in 1.2s. For a 25A step, the system reached steady-state in 1.4s. The response can be made faster by adjusting PI gains with a stability tradeoff. Figure 14 is provided to demonstrate how closely the experimental setup follows simulation results. Although both results settle at the commanded current, the differences lie towards the transient response. The simulated results demonstrate oscillations which can be explained by resonance due to including inductor resistance, DC-link capacitors, and dc source inductance. It does not model any additional capacitance and loop inductance in the circuit where the experimental setup may have. Figure 15 displays the steady-state response of this experiment. Note that there is a spike of current at every half-cycle, especially when referring to the diode or midpoint voltage, V_X, and diode current, i_D.

V. SUMMARY OF RESULTS

This work demonstrates the feasibility of utilizing SiC EL to estimate current from a SiC FET's body diode for classical power converter feedback control. The EL characteristics of SiC were explored to highlight its current and temperature dependency. When held at a constant junction temperature, the light intensity at the major peaks (390 nm and 500 nm) increases with rising current. This dependence on current arises from the injection of minority carriers into the PN-junction, thereby increasing radiative electron-hole recombination. At a constant current, but rising junction temperature, the 500 nm peak decreases while the 390 nm peak increases. The decrease in the 500 nm peak can be attributed to the increased thermal ionization of the donor level. The current and temperature have an interacting influence on the 390 nm peak where they both increase the light intensity. Whereas current and temperature counteract on the 500 nm peak where current increases light intensity while temperature decreases it. It is emphasized that these two influences are superimposed upon each other during regular operation. Due to this, a single intensity measurement will not sufficiently extract both current and temperature data accurately. To accurately control current in a buck converter implementing SiC EL, the simplest approach would be measuring the overall SiC EL spectra while controlling the temperature at a constant.

As mentioned in section II-C, it is possible to obtain a temperature reading from SiC EL through a 390 nm or a 500 nm bandpass filter and compare the intensity measurement to a set baseline intensity value at room temperature. However, provided that SiC is an indirect bandgap material, the EL emitted from SiC is very low in intensity compared to direct bandgap material wide bandgap semiconductors such as GaN, so it would require a substantial amount of current and heat to have SiC EL bright enough for a light transducer to pick up. This does not even take into account the transmissivity efficiency of a bandpass filter, which would further reduce the light intensity. However, there has been research to improve avalanche photodetectors for the visible light range. Authors in [42] developed an integrated APD for the visible light range with a high-speed response of 56 Gbps and a gain-bandwidth product of 234 GHz, achieving a gain of 10,000. With an APD capable of measuring low visible light intensity of SiC EL at adequate speeds, this approach could work.

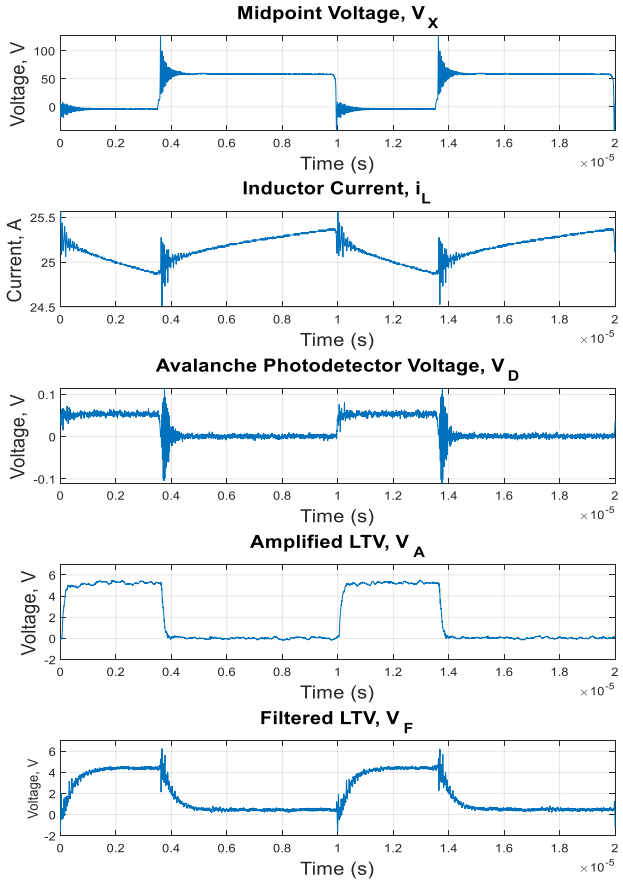

FIGURE 15. Steady-state waveforms of closed-loop control of SiC buck converter via EL feedback at 25A.

Another counterargument would be to implement a spectrometer into the system and use a large integration time. Then, use a baseline SiC spectra at room temperature to predict junction temperature. A neutral-network can be trained to perform this task as emphasized in [27], [28], and [29]. Unfortunately, that will not work in a control system where speed is paramount. As mentioned in section II-A, the integration time of the spectrometer was set to 30s to reasonably read the SiC EL spectra. It would require at least 30s to process the SiC EL spectra before predicting the system's current and temperature - that would be considered too slow for feasible applications. This approach could work if there is a spectrometer capable of measuring very low-light intensity EL at shorter integration times, but it is suspected that approach would be costly.

Due to challenges stemming from the low intensity of SiC EL, the optimal approach would involve measuring the overall SiC EL spectra while maintaining the junction temperature constant, preferably at room temperature or around 20°C. This way, a control system that incorporates SiC EL can be developed. An avalanche photodetector was used to measure SiC EL light intensity as an electrical signal. APDs have a larger noise floor due to avalanche noise, but they typically have better SNR due to their higher gains. However, APDs do behave nonlinearly at higher gains, which requires accurate calibration for SiC EL over a range of operating current and temperature. Calibration, which maps a relationship between system current and APD voltage, was performed by running a classical buck converter at 50% duty cycle and varying current. An external ADC was utilized to benefit from larger bit resolution, accommodate the filtered-amplified electrical signal of SiC EL with a larger acceptable input signal range, and achieve faster conversion speeds. The closed-loop system incorporates a classical PI controller that minimizes the error between commanded and measured current by regulating the system's duty cycle as illustrated in Figure 12. While the system's speed was capable of reaching steady-state in 1-1.4s s during a step response, this could be enhanced by adjusting the PI gains, albeit potentially compromising system stability. Another thing to note is the peaking during the on/off state of the buck converter is explained by the very high dV/dt and dI/dt of SiC as illustrated in Figure 10 and 15. Although this could be slightly suppressed by slowing down the rise time by increasing the gate resistance, this would increase the system's overall power loss and neutralize the benefits of SiC. Another problem is if the peaking is not adequately dealt with, provided that it is shared throughout the circuit, it could destroy a sensitive load with strict electrical limits. One additional thing to note is that because of SiC being an indirect bandgap material, the light emission is very weak and a typical APD is unable to detect SiC EL until around 5A as mentioned in section II-A. Due to this limitation, this system only works for higher current, higher power applications. Although alternative semiconductors that take advantage of their direct bandgap nature such as GaN can be used for lower current applications as demonstrated in [26]. Despite the limitations and potential problems of the proposed system, overall, it demonstrates the ability to control current of a system by measuring SiC EL. This type of control forms a basis of torque regulation in a motor drive, an ''inner-current'' loop of motor drive speed control, or even converter voltage control – as seen in classical closed-loop DC-DC converters that incorporates an inner-current loop through the use of hall-effect sensors [43], [44]. This system takes advantage of the characteristics and benefits of photons to replace the need for hall-effect sensors, where hall-effect sensor's accuracy and reliability is diminished by the effects of EMI.

The economic improvement of the proposed topology is comparable. Optical isolation through the use of fibers, avalanche photodetectors, and low-noise amplifiers results in an overall similar cost. This is assuming the average cost of fibers being tens of dollars per meter, an avalanche photodiode cost of tens to hundreds per unit, and low-noise amplifiers ranging from a couple cents to tens of dollars per IC depending on the specifications – all costs can be identified from typical providers such as Digikey and Mouser. Meanwhile, the average cost of an equivalent voltage and current sensors from providers such as LEM costs from tens to hundreds of dollars per unit. Despite an overall comparable cost, the greatest benefit is EMI immunity by benefiting off the characteristics of photons and fibers versus hall-effect

sensors where control system reliability and accuracy in high EMI environments is critical.

VI. CONCLUSION

In summary, this study demonstrates the potential of SiC EL for real-time current estimation in SiC FETs body diodes, offering benefits such as enhanced EMI immunity and potential cost savings. Despite challenges like low intensity emissions, SiC EL presents a promising alternative to traditional current sensing methods. Overall, this work marks a significant step towards more efficient and reliable power converter control systems for various industrial applications such as ''inner-current'' loop of motor drive speed control.

ACKNOWLEDGMENT

The authors would like to thank Subhashish Bhattacharya at NCSU for assistance in obtaining the SiC MOSFET modules.

REFERENCES

[1] S. K. Panda and A. Ghosh, ''A computational analysis of interfacing converters with advanced control methodologies for microgrid application,'' *Technol. Econ. Smart Grids Sustain. Energy*, vol. 5, no. 1, pp. 1–18, Dec. 2020.

[2] P. N. Babu, P. R. Bana, R. B. Peesapati, and G. Panda, ''An interleaved buck converter based active power filter for photovoltaic energy application,'' in *Proc. Int. Conf. Power Electron. Appl. Technol. Present Energy Scenario (PETPES)*, Mangalore, India, Aug. 2019, pp. 1–6.

[3] Y. U. Hong, S. H. Jung, Y. J. Woo, B. K. Choi, and G. H. Cho, ''Single-chip quasi-PWM DC–DC converter with fast transient response comprising loop-bandwidth control,'' *Electron. Lett.*, vol. 41, no. 8, p. 501, 2005.

[4] A. S. M. Antony and D. G. Immanuel, ''An overview of bootstrap converter for grid connected wind energy conversion system,'' in *Proc. 7th Int. Conf. Electr. Energy Syst. (ICEES)*, Chennai, India, Feb. 2021, pp. 515–523.

[5] Md. R. Haque, S. Das, M. R. Uddin, M. S. Islam Leon, and Md. A. Razzak, ''Performance evaluation of 1 kW asynchronous and synchronous buck converter-based solar-powered battery charging system for electric vehicles,'' in *Proc. IEEE Region 10 Symp. (TENSYMP)*, Dhaka, Bangladesh, Jun. 2020, pp. 770–773.

[6] S. Palanidoss and T. V. S. Vishnu, ''Experimental analysis of conventional buck and boost converter with integrated dual output converter,'' in *Proc. Int. Conf. Electr., Electron., Commun., Comput., Optim. Techn.*, Mysuru, India, Dec. 2017, pp. 323–329.

[7] S. N. Soheli, G. Sarowar, M. A. Hoque, and M. S. Hasan, ''Design and analysis of a DC–DC buck boost converter to achieve high efficiency and low voltage gain by using buck boost topology into buck topology,'' in *Proc. Int. Conf. Advancement Electr. Electron. Eng. (ICAEEE)*, Gazipur, Bangladesh, Nov. 2018, pp. 1–4.

[8] C. E. Sheridan, M. M. C. Merlin, and T. C. Green, ''Assessment of DC/DC converters for use in DC nodes for offshore grids,'' in *Proc. 10th IET Int. Conf. AC DC Power Transmiss. (ACDC)*, Dec. 2012, pp. 1–6.

[9] E. C. W. de Jong, J. A. Ferreira, and P. Bauer, ''Design techniques for thermal management in switch mode converters,'' *IEEE Trans. Ind. Appl.*, vol. 42, no. 6, pp. 1375–1386, Dec. 2006.

[10] K. Rasilainen, T. M. J. Nilsson, J. Bremer, M. Thorsell, and C. Fager, ''Thermal analysis of GaN/SiC-on-Si assemblies: Effect of bump pitch and thickness of SiC layer,'' in *Proc. 26th Int. Workshop Thermal Investigations ICs Syst. (THERMINIC)*, Berlin, Germany, Sep. 2020, pp. 249–253.

[11] K. Yamaguchi, ''Design and evaluation of SiC-based high power density inverter, 70 kW/liter, 50 kW/kg,'' in *Proc. IEEE Appl. Power Electron. Conf. Expo. (APEC)*, Long Beach, CA, USA, Mar. 2016, pp. 3075–3079.

[12] L. J. Petersen, D. J. Hoffman, J. P. Borraccini, and S. B. Swindler, ''Next-generation power and energy: Maybe not so next generation,'' *Nav. Eng. J.*, vol. 122, no. 4, pp. 59–74, Dec. 2010.

[13] L. J. Petersen and T. S. Ericsen, ''A history of silicon carbide (SiC) advancement: Basic research to product applications,'' *IEEE Transp. Electrific. Community*, Jun. 2017. [Online]. Available: https://tec.ieee.org/newsletter/june-2017/a-history-of-silicon-carbide-sic-advancement-basic-research-to-product-applications

[14] L. J. Petersen, M. Ziv, D. P. Burns, T. Q. Dinh, and P. E. Malek, ''U.S. Navy efforts towards development of future naval weapons and integration into an all electric warship (AEW),'' in *Proc. IMarEST Engine Weapon Int. Symp.*, Sep. 2011, pp. 1–16.

[15] T. Ericsen, ''Future navy application of wide bandgap power semiconductor devices,'' *Proc. IEEE*, vol. 90, no. 6, pp. 1077–1082, Jun. 2002.

[16] M. Vilathgamuwa, J. Deng, and K. J. Tseng, ''EMI suppression with switching frequency modulated DC–DC converters,'' *IEEE Ind. Appl. Mag.*, vol. 5, no. 6, pp. 27–33, Nov. 1999.

[17] B. Zhang and S. Wang, ''A survey of EMI research in power electronics systems with wide-bandgap semiconductor devices,'' *IEEE J. Emerg. Sel. Topics Power Electron.*, vol. 8, no. 1, pp. 626–643, Mar. 2020.

[18] W. Ma, Y. Wu, H. Li, and D. Chu, ''Investigation of the gate resistance and the RC snubbers on the EMI suppression in applying of the SiC MOSFET,'' in *Proc. IEEE Int. Conf. Mechatronics Autom. (ICMA)*, Aug. 2019, pp. 2224–2228.

[19] X. Wang, H. Pu, Q. Liu, L. An, X. Tang, and Z. Chen, ''Demonstration of 4H-SiC thyristor triggered by 100-mW/cm^2 UV light,'' *IEEE Electron Device Lett.*, vol. 41, no. 6, pp. 824–827, Jun. 2020.

[20] S. K. Mazumder and T. Sarkar, ''Optically activated gate control for power electronics,'' *IEEE Trans. Power Electron.*, vol. 26, no. 10, pp. 2863–2886, Oct. 2011.

[21] H. Riazmontazer and S. K. Mazumder, ''Optically switched-drive-based unified independent dv/dt and di/dt control for turn-off transition of power MOSFETs,'' *IEEE Trans. Power Electron.*, vol. 30, no. 4, pp. 2338–2349, Apr. 2015.

[22] M. A. Bryushinin, P. M. Karavaev, and I. A. Sokolov, ''Optically induced space-charge and conductivity gratings in wide-bandgap semiconductors,'' *Phys. Proc.*, vol. 86, pp. 136–140, Jan. 2017.

[23] L. Huang, C. Jiang, X. Zhao, and Y. Liu, ''Fabrication and sensing characteristics of 2 μm long period fiber grating written in double cladding fiber by CO_2 laser,'' in *Proc. 18th Int. Conf. Opt. Commun. Netw. (ICOCN)*, Huangshan, China, Aug. 2019, pp. 1–2.

[24] M. A. Porter, J. Williams, M. Broeg, K. Corzine, and T. Weatherford, ''Current and temperature measurement via spectral decomposition of light emission from a GaN power diode,'' in *Proc. IEEE Appl. Power Electron. Conf. Expo. (APEC)*, New Orleans, LA, USA, Mar. 2020, pp. 640–646.

[25] J. Piprek, ''Efficiency droop in nitride-based light-emitting diodes,'' *Phys. Status Solidi, A*, vol. 207, no. 10, pp. 2217–2225, 2020.

[26] J. D. Johnston, M. A. Porter, K. A. Corzine, and T. R. Weatherford, ''Closed-loop current control of a buck converter via sensing of optical emission from a GaN PN freewheeling diode,'' in *Proc. IEEE Appl. Power Electron. Conf. Expo. (APEC)*, Mar. 2023, pp. 2895–2900.

[27] S. Kalker, C. H. van der Broeck, and R. W. De Doncker, ''Utilizing electroluminescence of SiC MOSFETs for unified junction-temperature and current sensing,'' in *Proc. IEEE Appl. Power Electron. Conf. Expo. (APEC)*, Mar. 2020, pp. 1098–1105.

[28] L. A. Ruppert, S. Kalker, and R. W. De Doncker, ''Junction-temperature sensing of paralleled SiC MOSFETs utilizing temperature sensitive optical parameters,'' in *Proc. IEEE Energy Convers. Congr. Expo. (ECCE)*, Oct. 2021, pp. 5597–5604.

[29] S. Kalker, C. H. van der Broeck, L. A. Ruppert, and R. W. De Doncker, ''Next generation monitoring of SiC MOSFETs via spectral electroluminescence sensing,'' *IEEE Trans. Ind. Appl.*, vol. 57, no. 3, pp. 2746–2757, May 2021.

[30] H. J. Round, ''A note on carborundum,'' in *Semiconductor Devices: Pioneering Papers*, 1907. [Online]. Available: https://www.worldscientific.com/action/showCitFormats?doi=10.1142%2F9789814503464_0116

[31] J. Winkler, J. Homoth, and I. Kallfass, ''Utilization of parasitic luminescence from power semiconductor devices for current sensing,'' in *Proc. PCIM Eur., Int. Exhib. Conf. Power Electron., Intell. Motion, Renew. Energy Energy Manage.*, Jun. 2018, pp. 1–8.

[32] E. Schubert, ''Theory of radiative recombination,'' in *Light-Emitting Diodes*, 2nd ed. Cambridge, U.K.: Cambridge Univ. Press, 2006, pp. 48–58, doi: 10.1017/CBO9780511790546.004.

[33] A. Mikhail, A. Lebedev, N. Poletaev, A. M. StrelChuk, A. Syrkin, and V. E. Chelnokov, ''Deep centers and blue-green electroluminescence in 4H-SiC,'' *Semiconductors*, vol. 28, pp. 288–291, Jan. 1994.

[34] A. Yang, K. Murata, T. Miyazawa, T. Tawara, and H. Tsuchida, ''Time-resolved photoluminescence spectral analysis of phonon-assisted DAP and E—A recombination in N+B-doped n-type 4H-SiC epilayers,'' *J. Phys. D, Appl. Phys.*, vol. 52, no. 10, Mar. 2019, Art. no. 10LT01.

[35] A. A. Lebedev, "Deep level centers in silicon carbide: A review," *Semiconductors*, vol. 33, no. 2, pp. 107–130, Feb. 1999.
[36] A. A. Lebedev, B. Y. Ber, N. V. Seredova, D. Y. Kazantsev, and V. V. Kozlovski, "Radiation-stimulated photoluminescence in electron irradiated 4H-SiC," *J. Phys. D, Appl. Phys.*, vol. 48, no. 48, Dec. 2015, Art. no. 485106.
[37] P. B. Klein, "Long carrier lifetimes in n-type 4H-SiC epilayers," *Mater. Sci. Forum*, vols. 717–720, pp. 279–284, May 2012.
[38] N. I. Kuznetsov and A. S. Zubrilov, "Deep centers and electroluminescence in 4H SiC diodes with a p-type base region," *Mater. Sci. Eng., B*, vol. 29, nos. 1–3, pp. 181–184, Jan. 1995.
[39] A. Yang, K. Murata, T. Miyazawa, T. Tawara, and H. Tsuchida, "Time-resolved photoluminescence spectral analysis of phonon-assisted DAP and e–A recombination in N+B-doped n-type 4H-SiC epilayers," *J. Phys. D, Appl. Phys.*, vol. 52, no. 10, Mar. 2019, Art. no. 10LT01.
[40] S. Wen, W.-L. Zeng, C.-S. Lam, F. Maloberti, and R. P. Martins, "An analog multiplier controlled buck–boost converter," *IEEE Trans. Circuits Syst. II, Exp. Briefs*, vol. 69, no. 10, pp. 4173–4177, Oct. 2022.
[41] J. J. Gude and E. Kahoraho, "Modified Ziegler–Nichols method for fractional PI controllers," in *Proc. IEEE 15th Conf. Emerg. Technol. Factory Autom. (ETFA)*, Bilbao, Spain, Sep. 2010, pp. 1–5.
[42] S. Yanikgonul, V. Leong, J. R. Ong, T. Hu, S. Y. Siew, C. E. Png, and L. Krivitsky, "Integrated avalanche photodetectors for visible light," *Nature Commun.*, vol. 12, no. 1, p. 1834, Mar. 2021, doi: 10.1038/s41467-021-22046-x.
[43] Q. Tong, C. Chen, Q. Zhang, and X. Zou, "A sensorless predictive current controlled boost converter by using an EKF with load variation effect elimination function," *Sensors*, vol. 15, no. 5, pp. 9986–10003, Apr. 2015.
[44] O. Aiello, "Hall-effect current sensors susceptibility to EMI: Experimental study," *Electronics*, vol. 8, no. 11, p. 1310, Nov. 2019, doi: 10.3390/electronics8111310.

JOENY S. ZHEN (Student Member, IEEE) received the B.S.E.E. degree from California Polytechnic University, San Luis Obispo (Cal Poly), San Luis Obispo, CA, USA, in 2019, and the M.S. degree in electrical and computer engineering (ECE) from the University of California at Santa Cruz, Santa Cruz, CA, USA, in 2021. He is currently pursuing the Ph.D. degree in electrical and computer engineering with the Smart Power Laboratory, University of California at Santa Cruz. His current research interests include power electronics, reliability, power electronics control, radiation effects, pulsed power, drift step recovery diodes (DSRDs), and semiconductor opening switch (SOS) diodes. He has been working with the NIF&PS Target Area Science and Engineering Division (TASE) Group, Lawrence Livermore National Laboratory (LLNL), Livermore, CA, USA, for the past five years since summer 2020. He has been developing state-of-the-art pulsers for groups within NIF, where applications vary from flash X-ray cameras to particle accelerators.

KEITH A. CORZINE (Fellow, IEEE) received the Ph.D. degree from the University of Missouri–Rolla, Rolla, MO, USA, in 1997. He was with the University of Wisconsin–Milwaukee, and Missouri University of Science and Technology, and Clemson University. He is currently a Professor with the University of California at Santa Cruz. He held nine summer appointments with the Naval Surface Warfare Center, Philadelphia. He has authored or coauthored more than 70 refereed journal articles, more than 130 refereed international conference papers, and holds four U.S. patents related to power conversion. His research interests include power electronics, motor drives, naval ship propulsion systems, and electric machinery. He was the past IAS Chapter Officer of the IEEE Milwaukee Section and the past Chair of the IEEE St. Louis Section. He has also been involved in publicity and finance of IEEE conferences and served on the IEEE Region Five Audit Committee.

MATTHEW A. PORTER (Student Member, IEEE) received the B.S. degree in electrical and computer engineering from the United States Naval Academy, Annapolis, MD, USA, in 2010, and the M.S. degree in electrical and computer engineering from Naval Postgraduate School, Monterey, CA, USA, in 2011. He is currently pursuing the Ph.D. degree in electrical engineering with the Center for Power Electronics Systems, Virginia Tech, Blacksburg, VA, USA. His current research interests include wide bandgap power device fabrication and design, radiation effects in wide bandgap semiconductor devices, and power device reliability.

TODD R. WEATHERFORD (Senior Member, IEEE) received the B.S.E.E. degree from Rutgers University, New Brunswick, NJ, USA, in 1983, and the M.S.E.E. and Ph.D. degrees from North Carolina State University, Raleigh, NC, USA, in 1986 and 1992, respectively. He has held positions at Edmund Scientific, Barrington, NJ, USA; RCA Broadcast Systems, Camden, NJ, USA; RCA Advanced Technology Laboratories, Camden; and the Naval Research Laboratory, Washington, DC, USA. In 1995, he joined the Electrical Engineering Faculty, Naval Postgraduate School, Monterey, CA, USA, where he is currently a Professor with more than 100 graduate student theses. He has authored more than 80 publications in radiation effects, electronics, and device reliability. He is a member of the IEEE Reliability Society and the IEEE Nuclear and Plasma Sciences Society.